

Mechanical properties of 3D printed sandstone analogue with different binder rates

Minoru Sato

Central Research Institute of Electric Power Industry, Chiba, Japan

Takato Takemura

Geomechanics Lab., Department of Earth and Environmental Sciences, Nihon University, Tokyo, Japan

Daisuke Asahina

Geological Survey of Japan, AIST, Ibaraki, Japan

ABSTRACT: The mechanical properties of natural rocks obtained by laboratory tests vary considerably with rock anisotropy and heterogeneity by the formation process, and measurement accuracy of the equipment. However, it is difficult to evaluate these effects separately using natural rocks. Using three-dimensional (3D)-printed analogue minimizes the variations in the mechanical properties of rocks. In this study, the mechanical properties of 3D-printed sandstone analogues with different binder rates and jacketing conditions are examined at conventional triaxial compression (CTC) and true triaxial compression (TTC) stress conditions. This study demonstrates that the peak strength is slightly different for the same binder-sand weight rate samples; however, the deformation behavior observed from the shape of the stress–strain curve is similar. The mechanical properties and deformation behavior of the 3D-printed sandstone analogues are similar to those of natural sedimentary rocks under CTC and TTC testing conditions.

Keywords: 3D printing, sandstone, mechanical properties, true triaxial test, triaxial test, P-wave velocity.

1 INTRODUCTION

Understanding three-dimensional (3D) mechanical properties of rock around the tunnel is important for engineering projects. This knowledge is implemented in the evaluation of rock stability and tunnels of the excavation damaged zone. Therefore, various types of true triaxial test apparatus were recently established corresponding to simulated stress conditions (e.g., Nasser et al. 2014, Feng et al. 2016, Sato et al. 2018). The ISRM suggested method (Feng et al. 2019) was published to introduce guidelines for determining the deformation and failure characteristics of rocks subjected to true triaxial compression (TTC) on different stress paths. However, the results between different apparatuses and conventional laboratory testing methods, as well as different specimen sizes, aspect ratios, and shapes (cylindrical or rectangular prisms), heterogeneity of natural rocks cannot easily be verified. Therefore, using 3D-printed ground material analogue as a homogeneous specimen enables the comparison of mechanical properties from different testing methods. Osinga et al. (2015) reported that unconfined compressive strength tests on a 3D-printed rock analogue exhibit remarkably

consistent results in terms of peak strength, strain at failure, and Young's modulus. Subsequently, some studies have attempted to approximate the mechanical properties of natural sandstone using 3D-printed rock analogues. Different cases were considered by differing binder rates (Hodder et al. 2018) and increasing the density by incorporating a roller in the printing process (Hodder et al. 2020). However, the essential purpose of making a 3D-printed rock analogue is to confirm the results between different testing methods and/or conditions, the results of which have not yet been presented sufficiently.

In this study, the mechanical properties of 3D-printed sandstone analogues with different binder rates were examined at conventional triaxial compression (CTC) and TTC conditions. Furthermore, mechanical properties tested under different conditions of artificial sandstone were analyzed.

2 EXPERIMENTAL PROCEDURE

2.1 Materials

The 3D-printed sandstones comprised artificial granular mullite sand with a furfuryl alcohol binder. Sandstones were formed using high-speed additive manufacturing equipment (CMET Inc., SCM-10, Figure 1a). Binder jetting was performed using simple cylindrical and rectangular prismatic models designed via 3D CAD data (Figure 1b, c). The cylindrical specimens were $\phi 50 \times 100$ mm, and the rectangular prismatic specimens were $35 \times 35 \times 70$ mm. The binder rate was 2.4% in a weight ratio of sand when manufacturing a sand mold. The binder-sand weight rate was chosen as 2.4% from a previous study using 3D-printed sandstones formed by SCM-10 (Suzuki et al. 2018 and Okuzawa et al. 2018). However, it was extremely soft to calibrate the mechanical test apparatus for sandstones and/or bedrock. Therefore, the binder rates of 2.4% and 3.9% in the weight ratio of sand were chosen. Figure 1d shows the micrograph of a thin section of the 3D-printed sandstone with 2.4% binder rate. In rectangular prismatic specimens, the P-wave velocity was obtained in three directions.

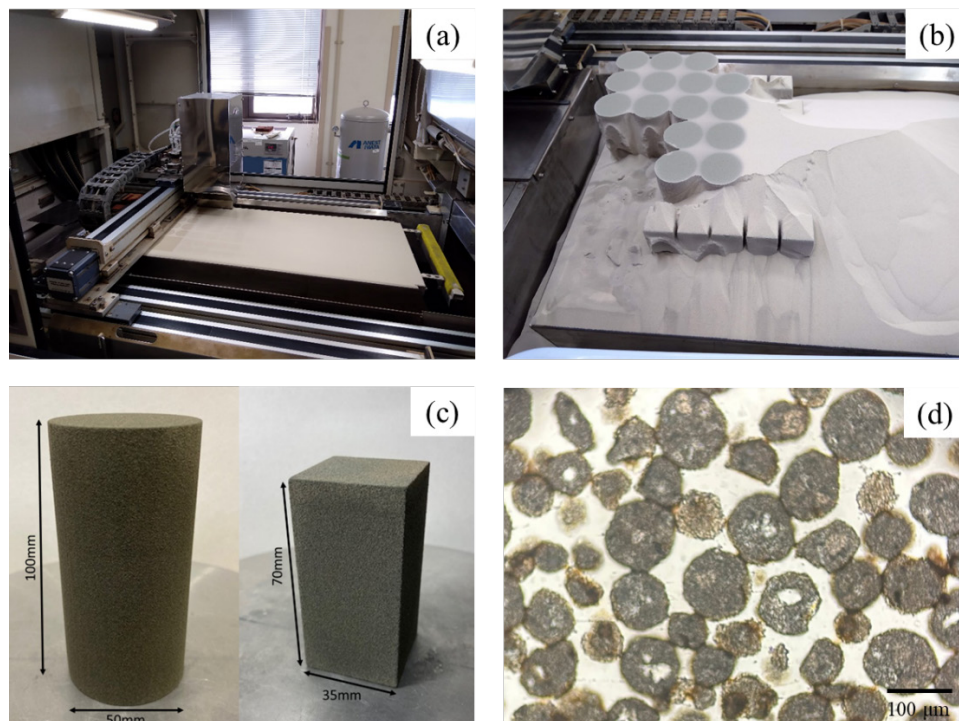


Figure 1. Overview of 3D printing, manufacturing, and sandstone analogues.

2.2 Mechanical and permeability properties of 3D printed sandstone analogues

Some studies have reported the mechanical and permeability properties of 3D printed sandstone (2.4% binder rate) analogues made using SCM-10. The uniaxial compressive strength was found to be 6.3 MPa (standard deviation is 0.32) from 10 specimens via uniaxial compression tests. The cohesion was 1.54 MPa, and the angle of internal friction was 27° ($R^2 = 0.67$) according to direct shear tests (Suzuki et al. 2018). For permeability properties, porosity was 49%, and the hydraulic conductivity was $(2.61 \pm 0.16) \times 10^{-4}$ m/s (Okuzawa et al. 2018). The variations in the permeability properties of the sandstone samples were low, whereas the mechanical properties obtained from laboratory tests under atmospheric pressure conditions exhibited variations.

2.3 CTC and TTC testing

CTC and TTC testing were conducted using the same apparatus (Figure 2). In this apparatus, maximum and intermediate stresses were applied through rigid pistons, and the minimum stress (confining pressure) was applied directly by oil pressure. The servo-controlled apparatus enabled three principal compressive stresses to be applied independently. When CTC was conducted, rigid pistons with intermediate stresses were detached from the specimen. The strain was obtained in three directions using a local deformation transducer (LDT).

In the CTC testing, the cylindrical specimen was placed between the endcaps and jacketed by a rubber or shrinkable tube (a fluoropolymer heat-shrinkable tube) to eliminate oil injected into the specimen. To decrease the effect of end friction, greased Teflon sheets were inserted between the specimen and endcaps. The axial stress (σ_1) was increased by a constant displacement rate (0.02 mm/min) under a constant confining pressure ($\sigma_3 = 2.5$ MPa).

In the TTC testing, a rectangular prismatic specimen was jacketed using silicone rubber. Greased Teflon and copper sheets were inserted between the specimen and endcaps. The confining pressure (σ_3) was maintained at 2.5 MPa. Subsequently, loading in the σ_2 and σ_1 directions was increased simultaneously by load control at approximately 5.0 MPa. Finally, the load along the σ_1 direction was increased at a constant displacement rate (0.02 mm/min) to the residual stress.

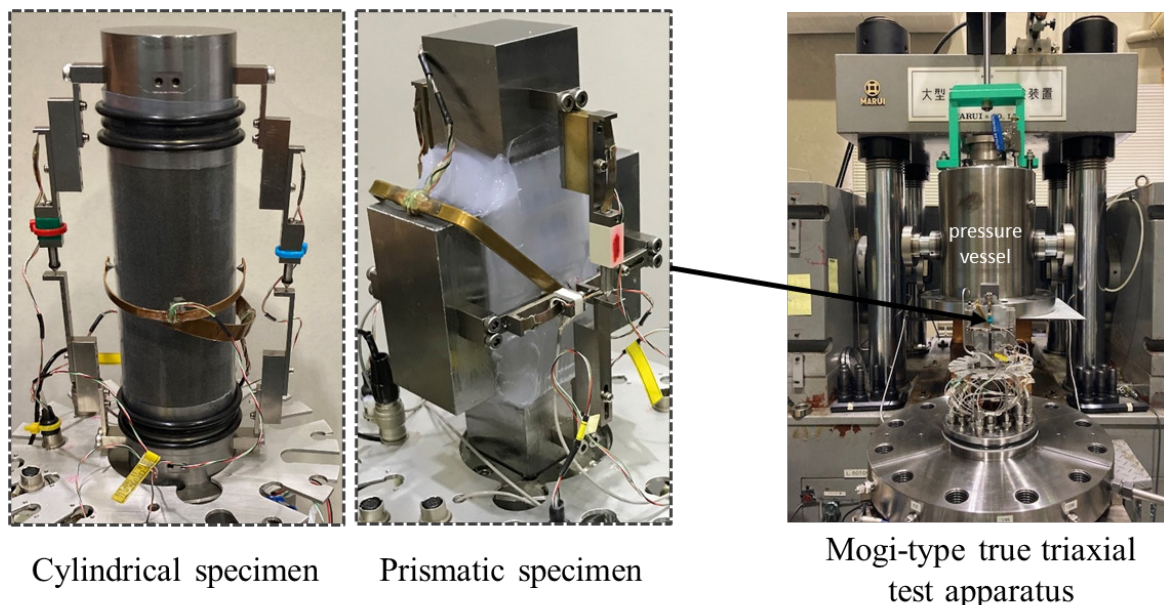


Figure 2. Photos of the true triaxial test apparatus and its assembly.

3 RESULTS

3.1 P-wave velocity

Table 1 shows the results of P-wave velocities in each of the three directions for rectangular primary specimens of AS2.4 and AS3.9; 2.4 and 3.9 denote the binder rates. V_{px} , V_{py} , and V_{pz} are the P-wave velocities in each direction, respectively. The Z-direction is in the axial direction (stacking direction), and the X- and Y-directions are perpendicular to each other. P-wave vibrators were calibrated to eliminate size effect of sample between vibrators. The result shows that V_{pz} is greater than V_{px} and V_{py} . Therefore, the P-wave velocity exhibited anisotropy caused by the stacking direction. The standard deviation of the P-wave velocity in all directions range from 0.03 to 0.04. Comparing AS2.4 and AS3.9, the P-wave velocity of AS3.9 is greater than that of AS2.4.

Table 1. P-wave velocities in each direction for (a) AS2.4 and (b) AS3.9 specimens (km/s).

(a)	V_{px}	V_{py}	V_{pz}	(b)	V_{px}	V_{py}	V_{pz}
AS2.4-1	1.92	1.94	2.13	AS3.9-1	2.06	2.03	2.27
AS2.4-2	1.92	1.89	2.15	AS3.9-2	2.01	2.08	2.38
AS2.4-3	1.91	1.86	2.08	AS3.9-3	2.04	2.09	2.32
AS2.4-4	1.86	1.83	2.06	AS3.9-4	2.03	2.09	2.27
AS2.4-5	1.86	1.90	2.11	AS3.9-5	2.14	2.15	2.39
AS2.4-6	1.92	1.88	2.11	AS3.9-6	2.09	2.05	2.26
AS2.4-7	1.91	1.89	2.07	AS3.9-7	2.12	2.11	2.31
AS2.4-8	1.91	1.85	2.08	AS3.9-8	2.10	2.08	2.30
Ave.	1.90	1.88	2.10	Ave.	2.07	2.09	2.31
S.D.	0.03	0.03	0.03	S.D.	0.04	0.03	0.04

3.2 CTC testing under different jacketing conditions

Figure 3 shows the results of CTC using membrane and shrinkable-tube jacketing. The peak and residual strengths in the shrinkable-tube jacketing condition were higher than those in the membrane jacketing condition. The results showed that the shrinkable tube strengthened the sandstone samples.

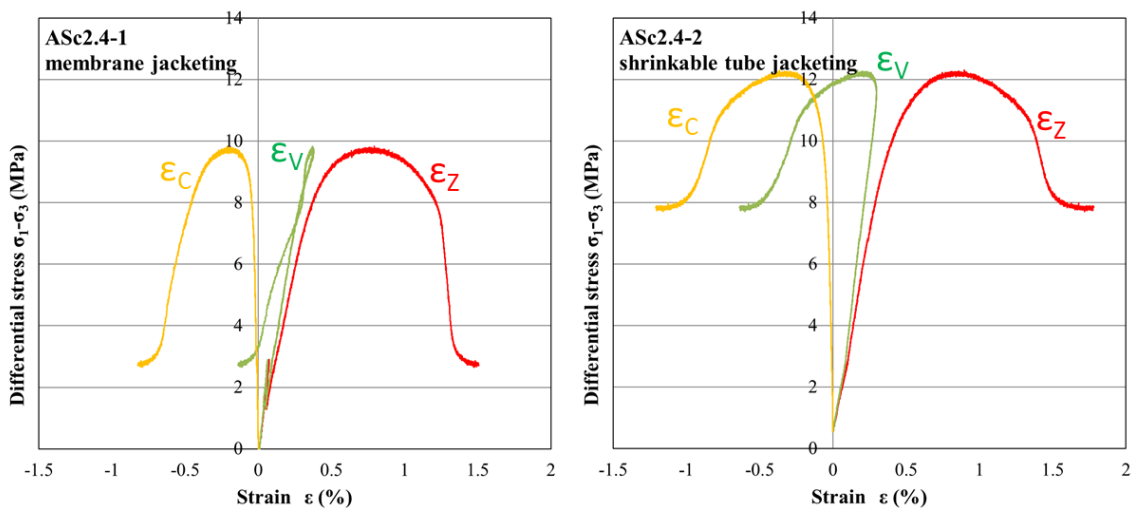


Figure 3. Stress–strain curves of different jacketing methods using membrane and shrinkable tube under same confining pressure (2.5 MPa) conditions.

3.3 Mechanical behavior of differential binder rate sandstone analogue

Figure 4 shows the stress–strain curves of differential binder rate samples under CTC (shrinkable tube jacketing) and TTC conditions. The peak strengths of the 3.9% binder rate samples were higher than those of the 2.4% binder rate samples. For the same binder rate samples (Figure 4b, red and blue lines), the peak strengths are slightly different. However, the shapes of the stress–strain curves are similar. Comparing the stress–strain curves of the same σ_3 and 2.4% binder rate, the CTC conditions exhibited ductile failure. In contrast, the TTC conditions exhibited brittle failure. The brittle–ductile transition affected by σ_2 was the same as that in a previous TTC study (Zhao et al. 2018). Figure 5 shows photographs from the σ_2 direction after TTC. The 2.4% binder-rate sample exhibited shear deformation, and the 3.9% binder-rate sample exhibited shear and split deformations. The shear and split planes of both the binder-rate samples were parallel to the σ_2 direction, and the samples expanded in the σ_3 direction by confining the σ_2 direction.

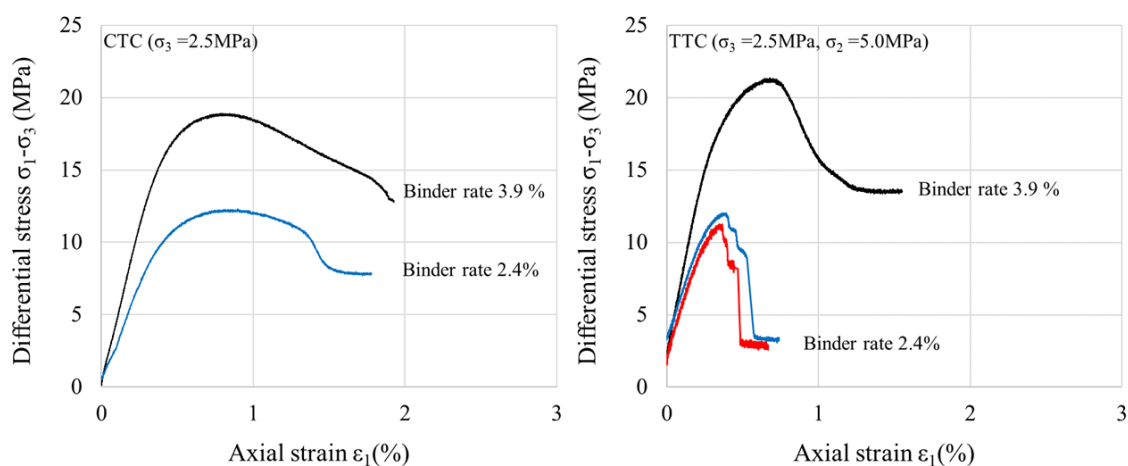


Figure 4. Mechanical behavior of differential binder-rate samples under CTC and TTC testing conditions.

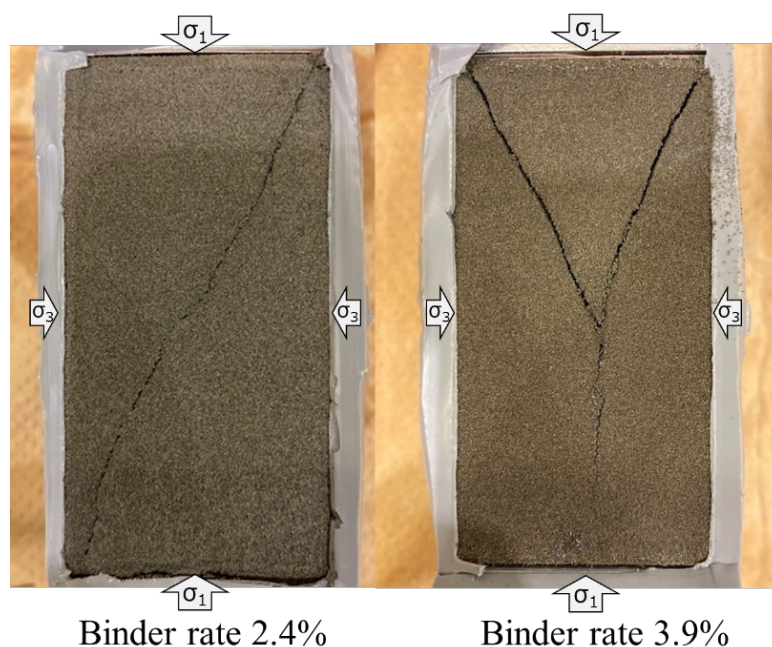


Figure 5. Photographs of TTC tested sample.

4 DISCUSSIONS

The CTC and TTC tests were performed under different binder-sand weight rates (2.4% and 3.9%) of 3D-printed sandstone analogues. The mechanical properties (P-wave velocity (Table 1), peak strength, and Young's modulus (Figure 4)) of the 3.9% binder-rate samples were higher than those of the 2.4% binder-rate samples. At the same binder rate, the peak strength was slightly different however, the shape of the stress–strain curve was similar under TTC testing. Comparing the two jacketing conditions under CTC testing showed that the peak and residual strengths of the shrinkable-tube jacketing condition were higher than those of the membrane jacketing condition. From the viewpoint of deformation behavior, the 2.4% binder-rate sample exhibited shear deformation, and the 3.9% binder-rate sample exhibited shear and split deformations. The shear and split planes of both binder-rate samples were parallel to the σ_2 direction, and the samples expanded in the σ_3 direction. The mechanical properties and deformation behavior of 3D-printed sandstone analogues are similar to those of natural sedimentary rocks under TTC testing conditions (e.g. Sato et al. 2018, Zhao, 2018). Furthermore, changes in the binder rate suggest the possibility of mimicking natural soft sandstones with specific mechanical properties. However, when a considerable amount of binder and unconfined compressive strength reach to plateau (Hodder et al. 2018), sufficient care is required. Using 3D-printed sandstone analogues as homogeneous specimens enabled the comparison of mechanical properties from different test conditions and methods.

REFERENCES

- Feng, X.T., Zhang, X, Kong, R. and Wang, G. 2016. A novel Mogi type true triaxial testing apparatus and its use to obtain complete stress-strain curves of hard rocks, *Rock Mechanics and Rock Engineering*, Vol. 49, pp. 1649-1662.
- Feng, X.T., Haimson, B., Li, X., Chang, C., Ma, X., Zhang, X., Ingraham, M. and Suzuki, K. 2019. ISRM Suggested Method: Determining deformation and failure characteristics of rocks subjected to True Triaxial Compression, *Rock Mechanics and Rock Engineering*, Vol. 52, pp. 2011-2020.
- Hodder, K., Nychka, J. A. and Chalaturnyk, R. J. 2018. Process limitation of 3D printing model rock, *Progress in Additive Manufacturing*, 3. pp. 173-182.
- Hodder, K., Ishutov, S., Sanchez, A., Zambrano, G. and Chalaturnyk, R. 2020. 3D printing of rock analogues in sand: a tool for design and repeatable testing of geomechanical and transport properties. *E3S Web of Conference, 2nd International Conference on Energy Geotechnics (ICEGT 2020)*, 205, DOI: 10.1051/e3sconf/202020504014
- Nasseri, M. H. B., Goodfellow, S. D., Lombos, L. and Young, R. P. 2014. 3-D transport and acoustic properties of Fontainebleau sandstone during true-triaxial deformation experiments, *International Journal of Rock Mechanics and Mining Sciences*, Vol. 69, pp. 1-18.
- Okuzawa, K., Hamamoto, S., Shimo, M. and Seiki, T. 2018. Transport properties of rock-like materials made by sand mold 3D printer equipment, *58th Japan National Conference on Geotechnical Engineering*, A-1, 0035. (in Japanese)
- Osinga, S. 2015. Study of geomechanical properties of 3D printed sandstone, *the 49th U.S. Rock Mechanics/Geomechanics Symposium, San Francisco, California, June 2015*, 15, 547.
- Sato, M., Takemura, T. and Takahashi, M. 2018. Development of the permeability anisotropy of submarine sedimentary rocks under true triaxial stresses, *International Journal of Rock Mechanics and Mining Sciences*, Vol. 108, pp. 118-127.
- Suzuki, K., Fujii, Y., Isobe, Y. and Sanoki, S. 2018. Shear strength of rock-like materials made by sand mold 3D printer equipment, *58th Japan National Conference on Geotechnical Engineering*, A-1, 0035. (in Japanese)
- Zhao, J., Feng, X. T., Zhang, X. W., Zhang, Y., Zhou, Y. Y. and Yang, C. X. 2018. Brittle-ductile transition and failure mechanism of Jinping marble under true triaxial compression, *Engineering Geology*, 232, 160-170.